Estimation of compact binary coalescense rates from short gamma-ray burst redshift measurements

Alexander Dietz*
LAPP, Université de Savoie, CNRS/IN2P3,
Chemin de Bellevue, BP 110,
74941 Annecy-le-Vieux CEDEX, France

Short gamma-ray bursts are believed to originate from the merger of two compact objects. If this scenario is correct, these bursts will be accompanied by the emission of strong gravitational waves, detectable by current or planned GW detectors, such as LIGO and Virgo. No detection of a gravitational wave has been made up to date. In this paper I will use a set of observed redshift measurements of short gamma-ray bursts to fit a model in order to determine the rate of such merger events in the nearby universe. Various corrections will be included in that calculation, as the field-of-view of the satellite missions, the beaming factors of gamma-ray bursts and other parameters. The computed rate estimations will be compared to other rate estimations, based on observations on binary neutron stars and population synthesis models. Given the upper limit established by LIGO/Virgo measurements, it is possible to draw conclusions on the beaming angle of gamma-ray bursts.

I. INTRODUCTION

Short gamma-ray bursts (GRB) are powerful explosions in the depth of the universe, probably created by the merger of two compact objects, like two neutron stars (NS-NS) or a neutron star and a black hole (NS-BH). Such events will be sources of strong gravitational waves (GW), which are being searched for with ground-based GW detectors such as LIGO and Virgo. Efforts have been made to estimate the local rates of such events, based on the observations of a few known neutron-star binary systems and on star population models. If short GRBs are indeed created by a merger of two compact objects, the observation of the redshift distribution can be used to determine the local merger rate in a complementary way, which is the main subject of this work. Furthermore, known limits on the rate of such events from LIGO/Virgo observations can be used to constrain parameters related to GRB physics, like the opening angle of the outflows in GRB.
This paper is organized as follows: After the introduction the available data on redshifts on short GRBs is reviewed, before the fit model is explained and the sources of uncertainties are discussed. Then the results of the calculations will be discussed, and compared with other rate estimations and the implications on GRB parameters.

A. Gamma-ray bursts

Gamma Ray Bursts are intensive bursts of high-energy gamma rays, distributed uniformly over the sky, lasting milliseconds to hundreds of seconds. Several thousands bursts have been discovered to date, with the very prominent feature of a bimodal distribution of the durations of the bursts, with a minimum around 2 seconds [1, 2]. Bursts with a duration shorter than 2 seconds are called short GRB's, and bursts lasting longer than 2 seconds are labelled long GRBs. Long GRB's have been associated with star-forming galaxies and core-collapse supernovae [3–7].
Short GRBs, on the other hand, had been a mystery for a long time, but recent observations indicate the progenitor of such events to be the merger of two compact objects [8, 9]. Especially observations from SWIFT contributed to that picture [10–12].
Besides the merger scenario, some of the short GRB's are probably caused by soft gamma repeaters (SGR), fast rotating magnetically-powered neutron stars, creating sporadic 'star quakes' in the crust which generate bursts of gamma radiation [13, 14]. It has been estimated that up to $\sim$25 % of all SGRB's are caused by SGR's [15, 16].
Throughout the remainder of this paper I will use a new GRB classification scheme suggested by Zhang *et.al.* [17], which labels a GRB with a probable merger progenitor as type-I GRB (i.e. the 'short'-GRB class) and GRB's which might have been created by a core collapse supernovae as type-II GRB (i.e. the 'long'-GRB class). Although this classification is not unambiguous (there are unclear cases like GRB 060614, or a sub-class might exist due to e.g. soft gamma-repeaters [18, 19]), this notation is based on the probable underlying physics instead of a single observational quantity, the duration of the burst.

*Electronic address: dietz@lapp.in2p3.fr

B. Associated gravitational wave observations

As mentioned just above, type-I GRBs might be sources of gravitational waves searched for with gravitational wave detectors, like LIGO and Virgo. The LIGO detectors, described in detail in [20, 21], consist of two instruments at two sites in the US, while Virgo consists of one instrument located near Pisa in Italy [22].
Several results on searches for merger signals have been published, with upper limits on the rates of merger events [23–27], along with triggered searches for merger signals associated with type-I GRBs [28, 29], but so far, no GWs have been detected. These detectors are currently undergoing significant enhancements, before a new data-taking campaign commences in $\sim$2015 with a 10-fold increase in sensitivity with respect to the initial configuration, probing a 1000-fold volume in space.

II. USED DATA AND REDSHIFTS

Because the redshifts are a very crucial piece of information in this work, I will re-examine the list of type-I GRBs associated with a redshift measurement in detail, to determine if the association is justified or not. Table I lists all 28 type-I GRBs with a possible redshift association; taken from [30, 31] and from diverse GCN circulars [32]. Each redshift association will be classified into three groups:

- **Reliable redshifts:** GRBs with a very large chance that the associated redshift is correct, which is the case when an optical counterpart was identified, or when only one galaxy is located in the error-circle of the observation. These GRB will be used in datasets labeled 'A' and 'B'.
- **Probable redshifts:** GRBs with a good chance that the redshift association is valid, in the case of e.g. two galaxies remaining in the error-circle, or when the observations lead to controversial results. These GRB will be used in dataset labeled 'B'.
- **Implausible redshifts:** GRBs with a very low probability that the assigned redshift is correct, as in the cases without identification of an optical counterpart or when many galaxies reside in the error circle. These GRBs will not be used in this analysis.

The following enumeration contains the very details on this re-examination, which is summarized in Table I:

a. GRB 020531 HETE detected this short GRB with a duration of 0.2-1 second [GCN1399][1] and followup observations revealed various sources in the IPN error circle [GCN1408,GCN1415] including two new asteroids [GCN1400]. One of these sources have been found to weaken in brightness [GCN1426], very close to an extended object, the probable host galaxy [GCN1427], with a spectroscopic redshift of z=1.0 [GCN1428]. Later, a different fading source was found just outside the error box [GCN1434], making this a probable redshift estimate only.
b. GRB 040924 This is a short GRB with a duration of $\sim$1.5 s [GCN2754] for which an optical afterglow (OA) has been identified [GCN2734]. A spectroscopic analysis of the very likely host galaxy [GCN2750] revealed a redshift of z=0.859 [GCN2800].
c. GRB 050416 This is a SWIFT/XRT GRB [GCN3264,GCN3268] with a duration of 2.4$\pm$0.2 seconds [GCN3273], and because an optical transient was observed [GCN3265,GCN3266] the measured redshift with z=0.6535$\pm$0.0002 [GCN3542] is very likely.
d. GRB 050509B GRB 050509B was found only within the XRT error circle [GCN3395] with a radius of 8". Further investigations showed that there are at least four more sources in the XRT error circle, one of them a probable high-redshift galaxy [GCN3401]. Although the chance association of a low redshift galaxy is reported to be very small [GCN3418], this redshift estimation is implausible.
e. GRB 050709 Although there is a long duration reported for this GRB of $\sim$130 seconds [GCN3653], the lightcurve and other spectral features classify it as a type-I GRB [GCN3570,GCN3653]. The association of the afterglow with the probable host galaxy [GCN3605,GCN3612] makes the redshift estimation of z=0.16 reliable.
f. GRB 050724 GRB 050724 has a T_{90} duration of strictly 3 ± 1 seconds, but because it could belong to the type-I GRB class [GCN3667] it is considered in the sample. Four objects has been found in the XRT error circle [GCN3672], of which 2 are identified as galactic stars [GCN3675,GCN3679]. Further observations made it very confident, that the object labelled as "D" is the host galaxy with a redshift of 0.258 [GCN3690,GCN3700].

---

[1] Each citation from the Gamma-ray Coordinate Netwok (GCN) will be given in this format. The citation can be found on the website `http://gcn.gsfc.nasa.gov/gcn3_archive.html`

g. GRB 050813 This SWIFT GRB with a duration of 0.6±0.1 seconds [GCN3793] has been found at a position with several faint extended objects, probably forming a galaxy cluster at high redshift, which makes this cluster the most likely source of that GRB [GCN3798]. Measurements of the redshift of the galaxies suggest a value of z=0.722 [GCN3801], although a redshift of z=0.65 also seems plausible [GCN3808]. The more conservative value of 0.722 will be used in this work as a probable value.
h. GRB 050906 SWIFT detected this very short GRB ($T_{90} = 0.128 \pm 0.016$s [GCN3935]) without finding the source within XRT, leaving only the BAT error circle to search for an afterglow [GCN3927,GCN3935]. Since this circle contains the massive star-forming galaxy IC 328 at z=0.031, a galaxy cluster at z=0.43 and field galaxies with unknown redshift, any value would be unlikely.
i. GRB 051016B For this SWIFT GRB with a duration of 4±0.1 s [GCN4104], a probable optical afterglow was found [GCN4111], in a galaxy with redshift z=0.9364 [GCN4186]; this makes the redshift value reliable.
j. GRB 051221A This GRB had a duration of 1.4±0.2 seconds [GCN4365], and an optical afterglow has been detected [GCN4375]. The measured redshift of z=0.5465 [GCN4384] is therefore reliable.
k. GRB 060502B GRB 060502B was a very short GRB with a duration of 0.09±0.02 seconds [GCN5064], for which two sources were found in the XRT error circle [GCN5066,GCN5071]. One is assumed to be a star while the other appears to an extended objects, whose reliable redshift is measured to be z=0.287 [GCN5238].
l. GRB 060505 This GRB has a nominal T_{90} duration time of 4 ± 1seconds [GCN5142], and therefore not clearly assigned to either type-I or type-II. The position of the optical afterglow was found to be 4".3 from the galaxy 2dFGRS S173Z112, with a redshift of z=0.089 [GCN5123]. The distance in projection of this late-type galaxy was found to be 7 kpc [GCN5123]. No supernova was detected associated with this GRB [GCN5161], suggesting that this might be either a merger-driven GRB or a

GRB	**instrument**	**Optical afterglow**	**duration [s]**	**redshift**	**classification**
020531	HETE	yes	1.0	1.0	probable
040924	**HETE**	**yes**	**$\sim$ 1.5**	**0.859**	**reliable**
050416	**SWIFT/XRT**	**yes**	**2.4±0.2**	**0.6535±0.002**	**reliable**
050509B	*SWIFT/XRT*	*no?*	*0.03*	*0.2248±0.0002*	*implausible*
050709	**HETE**	**yes**	**0.22±0.05**	**0.1606±0.0001**	**reliable**
050724	**SWIFT/XRT**	**yes**	**3.0±1.0**	**0.2576±0.0004**	**reliable**
050813	SWIFT/XRT	yes?	0.6±0.1	0.722	probable
050906	*SWIFT/BAT*	*no*	*0.128±0.016*	*0.43*	*implausible*
051016B	**SWIFT/XRT**	**yes**	**4.0±0.1**	**0.9364**	**reliable**
051221A	**SWIFT/XRT**	**yes**	**1.4±0.2**	**0.5465**	**reliable**
060502B	**SWIFT/XRT**	**no**	**0.09±0.02**	**0.287**	**reliable**
060505	SWIFT/XRT	yes	4±1	0.089	probable
060801	**SWIFT/XRT**	**no**	**0.5±0.1**	**1.131**	**reliable**
061006	**SWIFT/XRT**	**yes**	**130±10**	**0.4377±0.0002**	**reliable**
061201	**SWIFT/XRT**	**yes**	**0.8±0.1**	**0.111**	**reliable**
061210	*SWIFT/XRT*	*no*	*85±5*	*0.41*	*implausible*
061217	SWIFT/XRT	no	0.3±0.05	0.827	probable
070209	*SWIFT/BAT*	*no*	*0.10±0.02*	*0.314*	*implausible*
070406	*SWIFT/BAT*	*no*	*0.7±0.2*	*0.11*	*implausible*
070429B	**SWIFT/XRT**	**yes?**	**0.5±0.1**	**0.9023±0.0002**	**reliable**
070714B	**SWIFT/XRT**	**yes**	**64±5**	**0.9225±0.0001**	**reliable**
070724	SWIFT/XRT	no	0.4±0.04	0.457	probable
070810B	SWIFT/XRT	no?	0.08±0.01	0.49	probable
071227	**SWIFT/XRT**	**yes**	**1.8±0.4**	**0.384**	**reliable**
080121	SWIFT/XRT	no	0.7±0.2	0.046	probable
080520	**SWIFT/XRT**	**yes**	**2.8±0.7**	**1.545**	**reliable**
090417A	*SWIFT/BAT*	*no*	*0.072±0.018*	*0.088*	*implausible*
090510	**SWIFT/XRT**	**yes**	**0.3±0.1**	**0.903±0.003**	**reliable**

TABLE I: Set of 28 type-I gamma ray bursts with possible redshift measurements and T_{90} duration equal or less than 4 seconds. The data for these GRB's are taken from [30, 31] and from diverse GCN circulars (see [32]). Reliable redshift values are marked in **bold**, while implausible redshift values are marked in *italics*.

GRB at a much larger distance. The resdhift value is classified as probable.

m. GRB 060801 This short GRB (duration of 0.5±0.1 s [GCN5381]) was found in the SWIFT/XRT instrument [GCN5378], which revealed four objects in its field [GCN5384,GCN6386]. In the revised XRT error circle [GCN5389] two objects remained, of which one is extended. The redshift of that extended object is z=1.131 [GCN5470], making it a reliable estimation.

n. GRB 061006 An optical afterglow was found for this GRB [GCN5718], revealing the reliable redshift to be z=0.4377±0.0002 [33]. The formal duration is 130±10 s [GCN5704], but initial short spikes lasting ~ 0.5 seconds, on which SWIFT did not trigger [GCN5702,GCN5710], places this GRB into the type-I category.

o. GRB 061201 This short GRB (duration of 0.8 ± 0.1 seconds [GCN5882]) revealed an optical afterglow [GCN5896], but no galaxy at its position. Close-by objects include a galaxy at redshift 0.111 [GCN5952], as well as the galaxy cluster Abell 995, for which a mean redshift of z∼0.0835 was determined [GCN5995]. The offset of the GRB from the galaxy in the first case would be 34 kpc, while 800 kpc in the second case (from the center of the cluster). The value of z=0.111 is being used for the further analysis.[2]

p. GRB 061210 This GRB has a nominal duration of $T_{90} = 85 \pm 5$ s [GCN5905], but an initial short spike of duration ~ 60 ms and places it into the type-I regime. This GRB has been located in the XRT error circle containing three galaxies [GCN5922]. Since no optical transient was found, the association with a given galaxy as host is doubtable, which makes the redshift implausible.

q. GRB 061217 This short GRB, with a T_{90} of 0.30 ± 0.05 seconds [GCN5930], exhibited no optical afterglow, but the XRT position was found to be within 11 arcsec of a galaxy [GCN5948]. Two objects have been found in a more deeper observation, with the brighter object proposed to be the host galaxy of this GRB [GCN5949,GCN5953]. A subsequent observation of the proposed host galaxy yields a redshift of z=0.827 [GCN5965], so the source would have a isotropic-equivalent energy release of about 8×10^{49} erg [GCN5965], which is rather large for a type-I GRB. This makes the redshift probable only.

r. GRB 070209 The localization of this GRB within the BAT error circle contained no single source within the BAT error circle, but three X-ray sources in its proximity [GCN6095]. None of these sources were found to be the afterglow of this GRB [GCN6119], making the measured redshift of the source closest to the GRB position of z=0.314 [GCN6101] very unlikely.

s. GRB 070406 A short GRB with a T_{90} of 0.7 ± 0.2 seconds [GCN6261], for which a bright source was detected in the XRT error circle, whose redshift is 0.703 [GCN6262]. Spectral features indicate this to be a quasar, and unrelated to the burst. Further investigations showed no hint of a fading afterglow, and the majority of faint sources found in the XRT error circle make this redshift estimation of z=0.11 [GCN6249] very unlikely.

t. GRB 070429B This BAT GRB has a duration of 0.5 ± 0.1 s [GCN6365], and two faint objects were found in the XRT error circle [GCN6372]. For the brighter object a redshift of z=0.9023±0.0002 was determined [GCN7104][34], as well as an evidence that this object contains a fading source [GCN7145]. Therefore the measured redshift is reliable.

u. GRB 070714B This long GRB with a standard T_{90} time of 64±5 seconds shows spectral features of a type-I GRB, especially the zero spectral lag [GCN6623]. An optical transient was found in the XRT [GCN6630], and the host's galaxy redshift is found to be z=0.9225±0.0001 [GCN6836][34], which makes this a reliable redshift.

v. GRB 070724 This SWIFT GRB [GCN6654] had a duration of 0.4±0.04 seconds [GCN6656], and two sources were found in the XRT error circle, none of which showed variations [GCN6673]. The redshift of one of the source was found to be z=0.457 [GCN6665], making this a probable estimation.

w. GRB 070810B This is a short GRB with a duration of only 0.08±0.01 seconds [GCN6753]. Several possible sources has been identified in the XRT error circle, among them a nearby bright galaxy at z=0.0385 (source S1) and a cluster of galaxies at a redshift of z=0.49 [GCN6756] with a X-ray source (source S2 in [GCN6754]). In a latter observation the second source was not detected any more, making this the probable position of the afterglow with a redshift of 0.49.

x. GRB 071227 For this GRB a optical afterglow has been found [GCN7157] coinciding with the single source in the XRT error circle [GCN7151]. The redshift of z=0.384 [GCN7152,GCN7154] is therefore reliable.

y. GRB 080121 The only redshift reported for this GRB is z=0.046 for two galaxies in the BAT error circle [GCN7210]. In this field many other galaxies are present, which might belong to a group of galaxies [GCN7210]. Since no XRT position could be determined [GCN7209], the redshift value is probable.

z. GRB 080520 For this short GRB, with a duration of 2.8±0.7 seconds [GCN7761], an optical afterglow was found [GCN7753] for which a redshift of z=1.545 was determined [GCN7757]. This is a reliable redshift estimation.

aa. GRB 090417A This GRB, with a duration of 0.072±0.018 seconds [GCN9138], was found to be close to a low-redshift galaxy [GCN9134] with a redshift of 0.088 [GCN9136]. Since no optical afterglow has been found for this GRB, the redshift values are implausible.

---

[2] Using the value of 0.0835 changes the outcomes of the fits and the results of this work insignificantly - it is therefore safe to use a redshift value of 0.111.

bb. GRB 090510 For this short GRB, with a duration of 0.3±0.1 seconds [GCN9337] an optical afterglow has been found [GCN9338], which gives a reliable redshift of z=0.903 [GCN9353].

The summary of the classifications is listed in Table I, leaving 15 GRBs with a reliable redshift association (dataset 'A') and 7 additional GRBs with a probable redshift association (dataset 'B' with 22 data-points in total). The 6 GRBs with an implausible association are not further considered in this analysis. A bias might exist from favoring redshift estimations from nearby GRBs, since these are in general brighter and the underlying galaxy can be identified more easily - but this uncertainty is not taken into account.

III. DESCRIPTION OF THE FIT MODEL

This section describes the model used to fit the observed redshift values, and the parameters needed to convert the fit results into an astrophysical rate.

A. The fit model

This subsection describes the model used for the fit, which is a general model for the rate of astronomical objects as a function of their cosmological redshifts. Such models are described e.g. by Chapman [18, 35] and Guetta [36] and will be used to model the distribution of type-I GRBs. This model expresses the number of observable objects with a redshift smaller than some redshift z_*, and is given by:

$$N(z_*) = N_0 \int_0^{z_*} dz \, \frac{R(z)}{1+z} \, \frac{dV(z)}{dz} \int_{L_{min}(P_{lim},z)}^{L_{max}} \Phi(L) dL \; . \tag{1}$$

In this equation $N(z_*)$ is the number of type-I GRB above some minimum luminosity with a redshift smaller than z_*, $R(z)$ is the rate-function (in units per volume) at a redshift z, $\Phi(L)$ is the luminosity function and $dV(z)/dz$ is the volume of a co-moving shell at redshift z. Standard cosmology parameters are used: Ω_M=0.27, Ω_λ=0.73, and h=0.71. The rate function $R(z)$ describes the change of the intrinsic rate of objects as a function of redshift z, and all functions used for the fits are described in Appendix B. The luminosity function $\Phi(L)$ describes the distribution of sources as a function of their luminosity; they are given in Appendix C. The upper integration limit is set to $L_{max} = 10^{55}$ergs, while the lower limit depends on the threshold of the satellite and the redshift as follows:

$$L_{\rm min}(z) = \frac{4\pi}{1+z} \, D^2_{\rm lum}(z) \, P_{\rm lim} \; . \tag{2}$$

The detection threshold P_{lim} is taken for the SWIFT satellite, and is roughly $P_{lim} \approx 10^{-8}$ergs/cm^2 as can be seen in Figure 12 in [37].
The fit of the model is performed by a least-squares fitting function from the scipy module of python [38], which uses a modified version of the Levenberg-Marquardt algorithm to minimize a given function, which is the difference between the observed data and the fitted model. For each dataset, every possible combination of rate function and luminosity function is used in equation (1), yielding 16 different fit functions for each dataset. A Kolmogorov-Smirnov (KS) probability is calculated to estimate the goodness-of-fit of each of these fit functions, and only fits with a KS probability of more than 80 %are kept for further analysis. The norm of this equation, N_0, denotes the number density of GRBs at zero redshift. To obtain the local rate $r_{\rm local}$, one need to take into account the observing period ($T = 5$ years) and the fraction of type-I GRBs used for the fit, compared to the total number of type-I GRBs observed during this period. The latter correction factors are f =28/15 for dataset 'A' and f =28/22 for dataset 'B'. The local rate is given as:

$$r_{\rm local} = \frac{f \, N_0}{T} \; . \tag{3}$$

This yields the local, uncorrected rate, which has to be corrected for several effects, as described in the next subsection.

GRB	angle in degrees	beaming factor f_b^{-1} with correction
GRB 050709	$>$1.5 [43]	< 9000
GRB 050724	8-15[43], $>$25 [44]	< 30 or $\sim$90-300
GRB 051221A	4[45], 3.7 [46]	$\sim$1250 or $\sim$1470
GRB 061021	$4.5\zeta = 4.8$ [46]	$\sim$870

TABLE II: Table showing a list of opening angles or their lower limits. The beaming factors with correction are obtained from the angle by using $f_b^{-1} = 1/\left(1 - \cos(\frac{4}{7}\theta)\right)$; see text for details, including the definition of ζ.

B. Model dependent parameters

Several corrections must be applied to the local rate in order to obtain the true rate of binary mergers. These corrections include the beaming factor of GRBs f_b^{-1}, the field-of-view of the satellite υ, the fraction of mergers producing a type-I GRB, η, and the fraction of type-I GRBs created by a merger, σ. The general expression to obtain the true, corrected rate from the uncorrected, local rate is:

$$r_{\rm corr} = r_{\rm local} \frac{f_b^{-1}\,\sigma}{\eta\,\upsilon}\ . \tag{4}$$

1. *Beaming factor*

There has been convincing evidence that the outflows of GRBs are strongly beamed [39–42], which has to be considered in this work. Since gamma-ray bursts are only visible if the Earth is inside the cone of the outflow, the true rate will be higher than deduced from the redshift fits alone, by a factor $f_b^{-1} = 1/(1-\cos(\theta))$, the *beaming factor*. The angle θ is the opening angle of the outflow.
In the standard model of GRBs (see e.g. [47, 48] for recent reviews), the outflowing matter, initially having a Lorentz factor of Γ_0, is confined to a cone with opening angle θ. This changes, when the Lorentz factor of the outflow decelerates and becomes comparable to θ^{-1}; then the jet starts spreading sideways and an achromatic drop in the light curve (*jet-break*) is expected. Calculations have been performed on that matter, which show a dependency of the jet-break t_b on the jet opening angle as $\theta = 0.057\,\zeta\,t_b^{3/8}$ [49, 50], with ζ defined as

$$\zeta = \left(\frac{1+z}{2}\right)^{-3/8} \left(\frac{\eta_\gamma}{0.2}\right)^{1/8} \left(\frac{E_{\gamma,\rm iso}}{10^{53}\rm ergs}\right)^{-1/8} \left(\frac{n}{0.1\rm cm^{-3}}\right)^{1/8}\ . \tag{5}$$

Here z is the redshift of the source, η_γ the efficiency of converting the energy of the outflow into gamma rays, n is the mean circumburst density and $E_{\gamma,\rm iso}$ the isotropic equivalent gamma-ray energy.
It should be noted that the observer is in general not directly located on the jet axis, but forms an angle $\theta_{\rm off}$ relative to this axis [51], so that $\theta_{\rm meas} = \theta_{\rm true} + \theta_{\rm off}$. A typical observer is more likely located at a large angle off-axis, with a mean value of

$$\langle\theta_{\rm off}\rangle = \int_0^{\theta_{\rm true}} p(\theta)\,\theta\,d\theta = \frac{3}{4}\theta_{\rm true}\ , \tag{6}$$

having used the normalized probability density function $p(\theta) = 3\theta^2/\theta_{\rm true}^3$. The true average opening angle of a GRB is then given by

$$\theta_{\rm true} = \theta_{\rm meas} - \theta_{\rm off} \simeq \frac{4}{7}\theta_{\rm meas}\,, \tag{7}$$

which is only about half the angle as inferred by measurements of the jet-break times as explained above.

Evidence for jet-breaks in type-I GRBs are very rare, and summarized in Table II. The following list gives some more details on these findings:

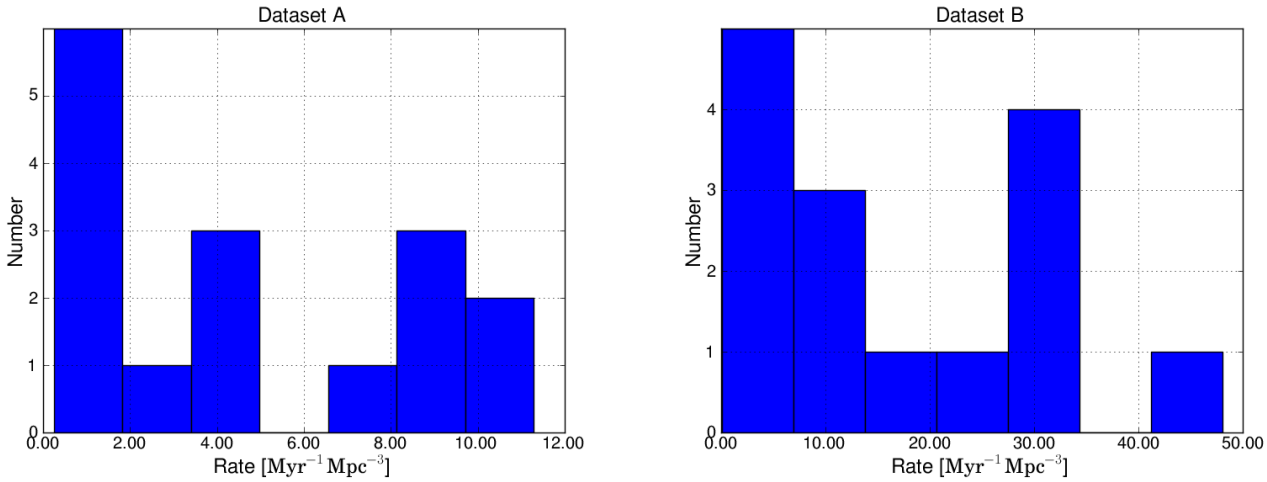

FIG. 1: Histogram of the fit results across the different rate functions and luminosity functions (as listed in Appendix A). The left plot shows the result for dataset 'A' (reliable redshift values), while the right plot shows the results for dataset 'B' (reliable and probable redshift values).

- **GRB 050709**: The afterglow of this GRB has been analyzed in [43] without having found a jet-break within 10 days after the time of the burst. Two different circumburst densities have been used ($n = 10$ cm^{-3} and $n = 10^{-5}$cm^{-3}), with the latter being more realistically in the case of a type-I GRB, yielding an opening angle of $\theta > 6°$ [43].
- **GRB 050724**: The afterglow for this GRB has also been analyzed by [43] with the claim of having seen a jet-break one day after the burst time, suggesting an opening angle of $\theta = 10 - 15°$ or a somewhat tighter value of $\theta = 8 - 12°$, assuming energy injected into the afterglow from long-lived X-ray flares [43]. The density was assumed to be in the range $n = 0.1 - 1000\,\mathrm{cm}^{-3}$. This result is doubted by [41]; they claim the opening angle to be larger than $25°$ for $n = 0.1\,\mathrm{cm}^{-3}$.
- **GRB 051221A**: The analysis of the lightcurve for this GRB yields three breaks, the last one accounted as the jet break for, corresponding to an opening angle of $\theta = 4°$ or $\theta = 8°$, depending on the ambient density ($n = 10^{-4}\,\mathrm{cm}^{-3}$ and $n = 0.1\,\mathrm{cm}^{-3}$, respectively) [42]. Again, the low-density value seems more appropriate for type-I GRBs. A value of $\theta = 3.7°$ is given in [46].
- **GRB 061021**: The jet-break times and the corresponding opening angles for this GRB can be found in [46], with an assumed circumstellar density of n$\simeq 1\,\mathrm{cm}^{-3}$. In the case of a type-I GRBs, however, the more probable place is a much less dense region, so a choice of n$\simeq 10^{-4}$cm^{-3} seems more appropriate. Using the mean redshift for type-I GRBs in equation (5) and a mean isotropic equivalent energy of $E_{\gamma,ISO} \simeq 10^{50}$ erg, a more realistic value for ζ=1.0573 has been used.

The findings of the opening angles of type-I GRBs are summarized in Table II, taking into account the correction factor of $4/7$. The beaming factors range between < 30 to up to $\sim$9000, which either represents the observational spread of the real value or hints to a multimodal distribution from different processes (i.e. SGR, NS-NS merger, NS-BH merger). In the remainder of this paper a value of f_b^{-1} =500 will be used, corresponding to an angle of 6.3°, which seem to be a reasonable choice and agrees with the range of $13 \lesssim f_b^{-1} \lesssim 10^4$ as found in [52, 53].

2. *Fraction of type-I GRB originating from a merger*

Not each type-I GRB will be caused by a merger event, some might be created from a soft-gamma repeater or a different process. As up to 25% of all type-I GRBs might be created by a SGR, an assumption that 75% have a merger progenitor seems reasonable; therefore a value of $\sigma = 0.75$ will be assumed in the remainder of this paper. Since this is the basic assumption on which this work is based, I will consider this a fixed value.

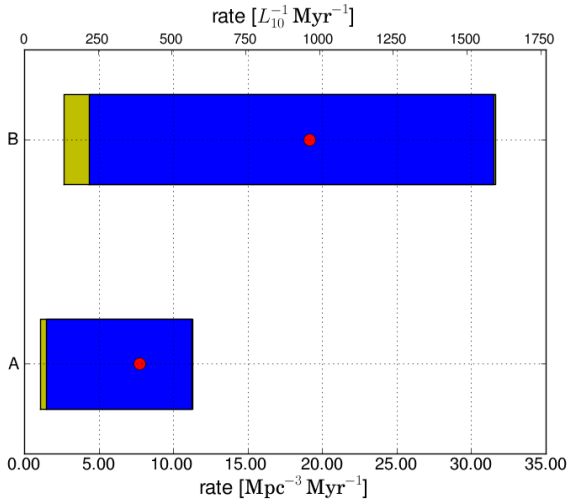

FIG. 2: Ranges for the computed rates using dataset 'A' with only the reliable redshift values and dataset 'B' with both, the reliable and the probable redshift values. The red dot indicates the median value, the blue bar the 20% to 80% quantile range, while the yellow bar covers the total rate range.

3. *Fraction of mergers producing a type-I GRB*

On the other side, not every merger will lead to a type-I GRB. One material object is needed to create the observed ultra-relativistic outflow, requiring one of the two objects to be a neutron star, while the other object can be either a neutron star or a black hole. Even then, it is hard to estimate the fraction of mergers that might create a type-I GRB; a recent investigation yield a number of $\eta = 0.01 - 0.4$ in the case of NS-BH systems [54], with an even larger spread in the case of NS-NS systems [55]. The recent discovery of a 2-Solarmass Neutron Star [56, 57] makes it much more plausible that two coalescing neutron stars are generating type-I GRBs [58], resulting in a much larger value for η. A value of $\eta = 0.5$ is being used in the remainder of this paper, but the effects of varying this parameter are investigated as well.

4. *Field-of-view*

Most of the GRBs considered in this work are detected by SWIFT, which has a field-of-view (FOV) of 1.4 sr half-coded [59]. This corresponds to about 10% visibility of the sky ($\upsilon = 0.1$) at any time for SWIFT. Although GRB data from other missions have been used[3], and the actual sky coverage is not constant, a value of 10% seems reasonable throughout the period considered in this paper. This also includes the assumption of a 100% duty cycle over the entire period of 5 years.

IV. FIT RESULTS AND DISCUSSION

With the discussion of the parameters in the previous section, it follows the true corrected rate $r_{\rm corr}$ is obtained from the uncorrected local rate $r_{\rm local}$ with the following expression:

$$r_{\rm corr} = 7500\, r_{\rm local} \left(\frac{f_b^{-1}}{500}\right) \left(\frac{\sigma}{0.75}\right) \left(\frac{0.50}{\eta}\right) \left(\frac{0.10}{\upsilon}\right) \tag{8}$$

in which the prefactor is just reflecting the default choices (and is equal to $500 \cdot 0.75/(0.50 \cdot 0.10)$).
Table IV in Appendix A summarizes the final sample of models, including their fitted parameters and the goodness-of-fit values, when using the parameters as shown in equation (8). For dataset 'A', the lowest rate (1.1 Myr^{-1} Mpc^{-3}) is obtained from the model with the delay rate function and power luminosity function, while the maximum rate (11.3 Myr^{-1} Mpc^{-3}) is obtained

[3] from HETE, http://space.mit.edu/HETE/

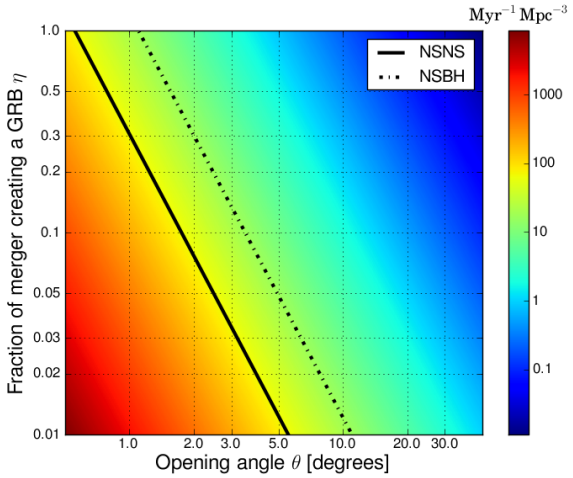

FIG. 3: Plot of the rate for model 'delay power', which yields the minimum rate (see Appendix B), as a function of the GRB opening angle θ and the parameter η. The other parameters are kept constant as they are more reliable. The color show the rate in units of Myr^{-1} Mpc^{-3}, and the black lines delineate the areas excluded by GW upper limits in the case of NS-NS and NS-BH binaries [60]; the lower left areas are excluded.

from the model with a constant rate function and lognormal luminosity function. The histogram of the rates are shown, for both datasets, in Figure 1, and in Figure 2 as a bar plot, indicating the 20%, 50% and 80% quantiles. For dataset 'B' the rates lie between 2.6 to 31.6 Myr^{-1} Mpc^{-3}. As dataset 'B' includes redshift values which are more uncertain and on average closer, it is not surprising this set yields larger rate values. To be conservative only results from dataset 'A' will be used in the remainder of this paper.

A. Constraints on GRB parameters

The effect of the uncertainty of the parameters f_b^{-1} and η is shown in Fig. 3, which shows the minimum rate obtained from a model (i.e. model 'delay power' in Appendix A), as a function of the opening angle θ and the fraction of mergers creating a type-I GRB, η. These lower limits vary between 0.01 Myr^{-1} Mpc^{-3} and 10^4 Myr^{-1} Mpc^{-3}, while the upper limits are between 0.1 Myr^{-1} Mpc^{-3} and 10^5 Myr^{-1} Mpc^{-3}. The black lines show the 90% upper limits on merger rates as a result of LIGO/Virgo searches, which are 43.6 Myr^{-1} Mpc^{-3} for NS-BH mergers and 172 Myr^{-1} Mpc^{-3} for NS-NS mergers [60]. The areas to the lower left of these lines are excluded which impose constraints on the opening angle θ on the outflow in GRBs. When assuming most type-I GRBs are created by NS-BH mergers an opening angle of less than $\sim 1^\circ$ is excluded. This plot also indicates that η might be not too small, agreeing with results obtained in [54, 58].

B. Comparison with other rate estimates

This section compares the rates deduced in this paper with other rates estimates. Two cases are considered: The coalescence rate of two neutron stars and the coalescence rate of a Neutron Star with a Black Hole. For NS-NS the rate is deduced from known binary pulsars in our Milky Way, and have been estimated to be realistically around 1 Myr^{-1} Mpc^{-3}, although they could be as high as 50 Myr^{-1} Mpc^{-3} [61]. The rates predicted for NS-BH are much more uncertain, and have been estimated using population synthesis models. Realistic rates are around 0.03 Myr^{-1} Mpc^{-3}, although they could be as high as 1 Myr^{-1} Mpc^{-3} [63].

The rates estimated in this work cover a range of 1.1 Myr^{-1} Mpc^{-3} to 11.3 Myr^{-1} Mpc^{-3}, with a median value at $\sim$7.8 Myr^{-1} Mpc^{-3} for the choice of plausible parameters as used at the beginning of this section. When including the uncertainties for the beaming factor f_b^{-1}, ranging from 30 (corresponding to 26°) to 9000 (corresponding to 1.5°), and for the fraction of mergers producing a type-I GRB η, from 0.01 to 1.0, the minimum rate becomes 0.03 Myr^{-1} Mpc^{-3}, while the maximum rate becomes 10200 Myr^{-1} Mpc^{-3}. Table III compares these rate estimations with the ones given in [61]. The plausible pessimistic rate estimation R_{low} is identified with the minimum rate from this work, and the realistic rate estimation R_{re} is identified with the median value estimated in this work using the plausible parameter choices. This value, $\sim$7.8 Myr^{-1} Mpc^{-3}, is very similar to the high rate estimation R_{high} for NS-NS mergers given in [61] (see Table III). It should be also noted that

	R_{low}	R_{re}	R_{high}	R_{max}
NS-NS ($\mathrm{Myr}^{-1}\,\mathrm{Mpc}^{-3}$)	0.01	1	10	50
NS-BH ($\mathrm{Myr}^{-1}\,\mathrm{Mpc}^{-3}$)	6×10^{-4}	0.03	1	
this work ($\mathrm{Myr}^{-1}\,\mathrm{Mpc}^{-3}$)	0.03	7.8	—	10^4
	R_{low}	R_{re}	R_{high}	R_{max}
NS-NS ($L_{10}^{-1}\mathrm{Myr}^{-1}$)	0.5	50	500	2500
NS-BH ($L_{10}^{-1}\mathrm{Myr}^{-1}$)	0.03	1.5	50	
this work ($L_{10}^{-1}\mathrm{Myr}^{-1}$)	1.5	390	—	5×10^5

TABLE III: Comparison of realistic rate estimations from this work with the estimations given in [61]. I identify R_{low} with the pessimistic estimation (the minimum rate obtained in this work), R_{pl} with the plausible estimate (the median rate obtained in this work), R_{high} with the plausible optimistic estimation and R_{max} with the upper limit (the upper limit in this work as well). The conversion factor between the two units is 0.0198 L_{10}/Mpc^3 [62].

the maximum rate estimation of 10200 $\mathrm{Myr}^{-1}\,\mathrm{Mpc}^{-3}$ is much larger than the excluded value from LIGO/Virgo measurements which are 43.6 $\mathrm{Myr}^{-1}\,\mathrm{Mpc}^{-3}$ for NS-BH mergers and 172 $\mathrm{Myr}^{-1}\,\mathrm{Mpc}^{-3}$ for NS-NS mergers [60]. For completeness Table III also shows the rates in units of $L_{10}^{-1}\mathrm{Myr}^{-1}$.

V. SUMMARY AND CONCLUSION

This work utilized redshift measurements of type-I GRBs (i.e. short GRBs) to obtain the local rate of NS-NS and NS-BH mergers, respectively. The list of available redshifts have been revisited in detail, to assess reliability of each redshift value. From the list of 22 type-I GRBs observed between 2004 and 2009, 15 have been found to be reliable, and 7 with probable values; the redshifts of the remaining 6 type-I GRB were found to be too uncertain and were excluded from the analysis.
A cumulative distribution has been constructed using the two datasets of redshift values, which have been fitted to models using different functions for the rate and luminosity. A KS-test criterion was used to select models with reliable good fits. To obtain the true local rate, the fit results have been corrected for several factors, including the fraction of mergers producing a type-I GRB, η, the number of type-I GRBs created by a merger and the beaming factor of the GRBs.
The obtained rates are consistent with the high-rate estimates given in [61], with a median rate of 7.8 $\mathrm{Myr}^{-1}\,\mathrm{Mpc}^{-3}$. When including the uncertainties from the beaming factor and parameter η, the rate is found to vary between 0.01 $\mathrm{Myr}^{-1}\,\mathrm{Mpc}^{-3}$ and 10^5 $\mathrm{Myr}^{-1}\,\mathrm{Mpc}^{-3}$. However, results from LIGO/Virgo observations, placing an upper limit on the rates of NS-NS and NS-BH mergers, can be used to constrain the opening angles of GRBs; the investigation indicates that opening angles with $\lesssim 1^\circ$ are excluded.
Further work is required to improve the accuracy on the results, i.e. by taking into account the fluxes measured for GRBs, or by constraining the ranges of some parameters used in this work. Ultimately, only direct detections of gravitational waves from mergers will yield a more precise rate, and if associated with type-I GRBs, physical properties of gamma-ray bursts can be constrained as well.

Acknowledgments

I would like to thank Chris Belczynski and Tomasz Bulik for providing many useful ideas and suggestion, and especially Frederique Marion and Benoit Mours for carefully reading this manuscript.

Appendix A: Full results

Data	Model	$\ln L_0$	α, σ	β	KS	Rate [$\mathrm{Mpc}^{-3}\mathrm{Myr}^{-1}$]
A	constant power	—	1.8	—	0.99	9.22
A	constant schechter	50.5	1.8	—	1.00	11.24
A	constant lognormal	24.1	8.1	—	1.00	11.29
A	sfr power	—	2.0	—	0.81	7.76
A	sfr schechter	49.3	1.9	—	1.00	9.20
A	sfr lognormal	45.3	2.5	—	1.00	8.59
A	merger power	—	2.2	—	0.81	2.94
A	merger schechter	49.4	2.2	—	1.00	3.99
A	merger lognormal	44.0	2.7	—	1.00	3.74
A	delay power	—	2.3	—	0.95	1.07
A	delay schechter	49.8	2.3	—	1.00	1.49
A	delay lognormal	35.5	4.6	—	1.00	1.47
B	constant power	—	1.9	—	0.99	23.91
B	constant schechter	55.1	1.9	—	0.96	31.28
B	constant lognormal	-510.2	37.0	—	0.96	31.25
B	sfr power	—	2.1	—	0.94	19.12
B	sfr schechter	54.4	2.2	—	1.00	31.60
B	sfr lognormal	-383.5	28.7	—	1.00	31.51
B	merger power	—	2.3	—	0.94	7.04
B	merger schechter	55.3	2.4	—	1.00	13.30
B	merger lognormal	-317.1	24.2	—	1.00	13.27
B	delay power	—	2.3	—	1.00	2.63
B	delay schechter	55.7	2.5	—	0.98	4.37
B	delay lognormal	-316.0	23.9	—	0.98	4.35

TABLE IV: Table containing the fit results with a KS-probability of at least 80 %which have been used in this work. The value for L_0 are given in units of $\log_{10}$. The actual values of L_0 associated with the schechter luminosity function are irrelevant, as they exhibit a large variation in σ. Note, that no model using a broken power law gives a sensible fit (and therefore the β column is empty).

Appendix B: Rate models

This section describes the rate functions which are used to fit the data according to eq. (1), except for the trivial case of the '**constant**' rate.

1. The '**sfr**' rate that follows the star formation rate (model 'SF2') described in [36, 64]:

$$R(z) \equiv R_{SF2}(z) = R_{s,0} \frac{23 \exp(3.4\, z)}{\exp(3.4\, z) + 22} \tag{B1}$$

2. The '**merger**' rate that follows merger rate of two compact objects, as derived in [36] from six observed double neutron stars [65]. This rate is following a time-delay distribution ($\propto 1/\tau$):

$$R(z) = R_{M,0} \int_0^{t(z)} d\tau\, R_{SF2}\left(z(t-\tau)\right)/\tau \tag{B2}$$

3. The '**delay**' rate similar to the 'merger' rate, but with a *constant* time-delay distribution :

$$R(z) = R_{D,0} \int_0^{t(z)} d\tau\, R_{SF2}\left(z(t-\tau)\right)\ . \tag{B3}$$

Appendix C: Luminosity models

This section describes the luminosity functions which are used to fit the data according to eq. (1).

1. A **single power law** distribution, which is often used to describe the pdf of luminosity in astrophysics (with two parameters: Φ_0 and α):

$$\Phi(L) = \Phi_0 \left(\frac{L}{L_0}\right)^{-\alpha} \tag{C1}$$

2. A **broken power law** distribution, describing e.g. two underlying populations in the luminosity [36] (with four parameters: Φ_0, L_0, α and β):

$$\Phi(L) = \Phi_0 \left(\tfrac{L}{L_0}\right)^{-\alpha} \quad \text{for } L < L_0 \tag{C2}$$

$$\Phi(L) = \Phi_0 \left(\tfrac{L}{L_0}\right)^{-\beta} \quad \text{for } L >= L_0 \tag{C3}$$

3. The **Schechter distribution**, as used for example in ref [66] (with three parameters: Φ_0, L_0 and α):

$$\Phi(L) = \Phi_0 \left(\frac{L}{L_0}\right)^{-\alpha} \exp(-L/L_0) \tag{C4}$$

4. The **log-normal distribution**, describing a standard candle, e.g. a population with about the same luminosity (following [18], with three parameters: Φ_0, L_0 and σ):

$$\Phi(L) = \Phi_0 \frac{1}{L} \exp\left(\frac{-(\log L - \log L_0)^2}{2\sigma^2}\right) \tag{C5}$$

[1] C. Kouveliotou et al. Astrophys. J. **413**, L101 (1993).
[2] I. Horvath, A&A **392**, 791 (2002), arXiv:astro-ph/0205004.
[3] S. Campana et al., Nature **442**, 1008 (2006).
[4] W. H. Lee, E. Ramirez-Ruiz, and D. Page, Astrophys. J. **608**, L5 (2004), arXiv:astro-ph/0404566.
[5] J. Hjorth et al., Nature **423**, 847 (2003).
[6] A. S. Fruchter, Nature **441**, 463 (2006).
[7] S. E. Woosley and J. S. Bloom, Ann. Rev. of Astron. and Astroph. **44**, 507 (2006).
[8] D. Eichler, M. Livio, T. Piran, and D. Schramm, Nature **340**, 126 (1989).
[9] R. Narayan, Paczynski, and T. Piran, Astroph. J. **395**, L83 (1992).
[10] URL `http://swift.gsfc.nasa.gov/docs/swift/swiftsc.html`.
[11] N. Gehrels et al., Nature **437**, 851 (2005).
[12] S. D. Barthelmy et al., Nature **438**, 994 (2005).
[13] S. Mereghetti, Astron. Astrophys. Rev. **15**, 225 (2008), arXiv:0804.0250 [astro-ph].
[14] P. M. Woods and C. Thompson, in *Compact Stellar X-Ray Sources*, edited by W. G. H. Lewin and M. van der Klis (Cambridge Univ. Press, Cambridge, 2004).
[15] N. R. Tanvir et al., Nature **438**, 991 (2005), arXiv:astro-ph/0509167v3.
[16] A. J. Levan et al., Mon.Not.Roy.Astron.Soc. **384**, 541 (2008), arXiv:0705.1705v1 [astro-ph].
[17] B. Zhang et al., The Astrophysical Journal **703**, 1696 (2009)
[18] R. Chapman, R. S. Priddey, and N. R. Tanvir (2008), arXiv:0802.0008 [astro-ph].
[19] B. Czerny, A. Janiuk, D. B. Cline, and S. Otwinowski, New Astron. **16**, 33 (2011), arXiv:1006.1470 [astro-ph.HE].
[20] B. Abbott et al. (LIGO Scientific Collaboration), Nucl. Instrum. Methods **A517**, 154 (2004).
[21] B. C. Barish and R. Weiss, Phys. Today **52 (Oct)**, 44 (1999).
[22] F. Acernese et al., Class. Quant. Grav. **23**, S635 (2006).
[23] B. Abbott et al. (LIGO Scientific Collaboration), Phys. Rev. D **69**, 122001 (2004), arXiv:gr-qc/0308069v1.
[24] B. Abbott et al. (LIGO Scientific Collaboration), Phys. Rev. D **72**, 082001 (2005), arXiv:gr-qc/0505041.
[25] B. Abbott et al. (LIGO Scientific Collaboration), Phys. Rev. D **72**, 082002 (2005), arXiv:gr-qc/0505042.
[26] B. Abbott et al. (LIGO Scientific Collaboration), Phys. Rev. D **73**, 062001 (2006), arXiv:gr-qc/0509129.
[27] B. Abbott et al. (LIGO Scientific Collaboration), Phys. Rev. D **77**, 062002 (2007), arXiv:0704.3368v4 [gr-qc].
[28] B. Abbott et al. (LIGO Scientific Collaboration), Astrophys. J. **681**, 1419 (2008), arXiv:0711.1163 [astro-ph].
[29] J. Abadie et al. (LIGO Scientific Collaboration), Astrophys. J. **715**, 1453 (2010), arXiv:1001.0165 [astro-ph.HE].
[30] R. W. O'Shaughnessy, V. Kalogera, and K. Belczynski, Astrophys. J. **675**, 566 (2008), arXiv:0706.4139 [astro-ph].
[31] T. Sakamoto et al. (2007), arXiv:0707.4626v3 [astro-ph].
[32] URL `http://gcn.gsfc.nasa.gov`.
[33] E. Berger, et al., Astrophys. J. **664**, 1000 (2007)
[34] S. B. Cenko et al. (2008), arXiv:0802.0874 [astro-ph].
[35] R. Chapman, R. S. Priddey, and N. R. Tanvir, AIP Conf. Proc. **983**, 304 (2008), arXiv:0709.4640 [astro-ph].
[36] D. Guetta and T. Piran (2005), arXiv:astro-ph/0511239v2.
[37] T. Sakamoto et al., Astrophys. Journal Suppl. Series **175**, 179 (2008), arXiv:0707.4626v3 [astro-ph].
[38] URL `http://www.scipy.org/`.
[39] K. Z. Stanek, P. M. Garnavich, J. Kaluzny, W. Pych, and I. Thompson, Astrophys. J. Lett. **522**, L39 (1999)
[40] F. A. Harrison, et al., Astrophys. J. Lett. **523**, L121 (1999)
[41] D. Grupe et al., Astrophys. J. **653**, 462 (2006), arXiv:astro-ph/0603773.
[42] D. N. Burrows et al., Astrophys. J. **653**, 468 (2006), arXiv:astro-ph/0604320.
[43] A. Panaitescu, Mon.Not.Roy.Astron.Soc.Lett. **367**, L42 (2006), arXiv:astro-ph/0511588
[44] D. Grupe, et al., Astrophys. J. **653**, 462 (2006), arXiv:astro-ph/0603773
[45] D. N. Burrows, et al., Astrophys. J. **653**, 468 (2006)
[46] J. L. Racusin et al., Astrophys. J. **698**, 43 (2009), arXiv:0812.4780 [astro-ph].
[47] T. Piran, Rev. Mod. Phys. **76**, 1143 (2005).
[48] P. Mészáros, Rep. Prog. Phys. **69**, 2259 (2006).
[49] R. Sari, T. Piran, and J. P. Halpern, Astrophys. J. Lett. **519**, L17 (1999)
[50] D. A. Frail et al., Astrophys. J. Lett. **562**, L55 (2001)
[51] H. van Eerten, W. Zhang, and A. MacFadyen (2010), arXiv:1006.5125 [astro-ph.HE].
[52] A. M. Soderberg, E. Nakar, E. Berger, and S. R. Kulkarni, Astrophys. J. **638**, 930 (2006)
[53] A. Levinson, E. O. Ofek, E. Waxman, and A. Gal-Yam, Astrophys. J. **576**, 923 (2002).
[54] K. Belczynski, R. E. Taam, E. Rantsiou, and M. van der Sluys (2007), arXiv:astro-ph/0703131.
[55] K. Belczynski, R. OShaughnessy, V. Kalogera, F. Rasio, R. E. Taam, and T. Bulik, Astrophys. J. Lett. **680**, L129 (2008), arXiv:0712.1036 [astro-ph]
[56] P. B. Demorest, T. Pennucci, S. M. Ransom, M. S. E. Roberts, and J. W. T. Hessels, Nature **467**, 1081 (2010)
[57] P. Demorest, T. Pennucci, S. Ransom, M. Roberts, and J. Hessels (2010), arXiv:1010.5788 [astro-ph.HE].
[58] F. Ozel, D. Psaltis, S. Ransom, P. Demorest, and M. Alford (2010), arXiv:1010.5790 [astro-ph.HE].
[59] S. D. Barthelmy et al., Space Science Reviews **120** (2005), arXiv:astro-ph/0507410.

[60] LIGO Scientific Collaboration and Virgo Collaboration (2010), arXiv:1005.4655 [gr-qc].
[61] LIGO Scientific Collaboration and Virgo Collaboration, Class. Quant. Grav. **27** (2010), arXiv:1003.2480 [astro-ph.HE].
[62] R. K. Kopparapu et al., Astroph. J. **675**, 1459 (2008), arXiv:0706.1283 [astro-ph].
[63] R. O'Shaughnessy, C. Kim, V. Kalogera, and K. Belczynski, Astrophys. J. **672**, 470 (2008).
[64] C. Porciani and P. Madau, Astrophys. J. **548**, 522 (2001).
[65] D. J. Champion et al., Monthly Notices RAS **350**, L61 (2004).
[66] S. Andreon, J.-C. Cuillandre, E. Puddu, and Y. Mellier, Mon.Not.Roy.Astron.Soc. **372**, 60 (2006), arXiv:astro-ph/0606710v1.